Low-Complexity Single-Layer Dual-Band Microstrip Patch Antenna for WiFi 6/6E Communication Systems

Tu Le-Tuan, Hien Nguyen-Thi, Nguyen Tran, and Hyun-chang Park, *Member, IEEE*

***Abstract*—This paper presents a dual-band patch antenna operating at 5.2 and 6.6 GHz for WiFi 6/6E communication systems. Unlike conventional approaches based on higher-order modes or stacked structures, which often lead to larger size and complicated structure, the proposed design employs two closely spaced patches of different sizes printed on the same layer to realize dual-band operation. These patches are capacitively excited through a probe-fed microstrip line located at the center, enabling a single-layer, low-profile, and low-complexity configuration. The optimized antenna occupies an overall size of $0.52\,\lambda \times 0.52\,\lambda \times 0.03\,\lambda$ at the lowest operating frequency of 5.2 GHz. The measured impedance bandwidths are 6.1% (5.12–5.44 GHz) and 4.9% (6.40–6.72 GHz) for the lower and upper bands, respectively. Within these bands, the antenna achieves measured peak gains in the broadside direction of 7.0 and 6.7 dBi, while maintaining stable and desirable radiation characteristics across both operating frequencies. Owing to its compact size and good operating characteristics, the proposed antenna is suitable for WLAN access points, IoT devices, and compact wireless terminals.**

Link to graphical and video abstracts, and to code:
https://latamt.ieeer9.org/index.php/transactions/article/view/10762

***Index Terms*—Dual-band antenna, Microstrip patch antenna, Single-layer, WiFi 6/6E, Low complexity.**

I. Introduction

To fully exploit the high channel capacity of Wi-Fi 6/6E systems, a dual-band antenna covering both 5 GHz and 6 GHz bands is highly required, since it enables simultaneous multi-stream transmission over wider spectrum resources while maintaining compatibility with Wireless Local Area Network infrastructure.

Dual-band operation with compact size and wide bandwidth can be conveniently realized with monopole structure [1], [2], but low gain radiation. Alternatively, a combination of dipole and artificial ground structure can produce dual-band radiation with high gain [3], [4]. However, very high profile is the critical drawback of this antenna type, which cannot be integrated into small devices. Microstrip patch antenna is the best solution to achieve dual-band operation with high gain and low-profile structure.

A widely adopted approach for achieving dual-band operation is to exploit multiple resonant modes within a single radiator [5]–[8]. However, the higher-order mode is usually associated with a substantially larger electrical size than the fundamental mode and may exhibit radiation characteristics that deviate from the desired beam profile. As a result, additional optimization or auxiliary structures are often required to ensure acceptable radiation performance. In general, such techniques inevitably involve trade-offs among antenna compactness, profile, and structural simplicity. Another commonly reported strategy is to employ multiple resonators tuned to different frequencies in a vertically stacked configuration [9]–[12], such as cascaded patch elements operating at separate bands. Although this approach can effectively realize dual-band functionality, it generally increases the antenna thickness due to the multilayer arrangement and introduces additional fabrication complexity.

To overcome these limitations, several single-layer dual-band antenna configurations have been reported. In [13]–[15], multiple resonant modes are exploited to achieve operation at two distinct frequency bands. In [16], multiple U-shaped slots are embedded into the radiating patch to generate dual resonances, whereas in [17], a defected ground structure (DGS) is introduced for dual-band operation. Another effective approach is to place separate radiators within the same layer in close proximity to the driven patch [18]–[21]. Although these designs can successfully realize dual-band functionality, they still suffer from several limitations, including relatively large size, low gain, narrow bandwidth, or unbalanced radiation performance between the two operating bands.

This paper proposes a dual-band patch antenna with single-layer, low-complexity, and balanced performance at two operating bands. The proposed antenna realizes dual-band behavior by employing two closely spaced patches with different dimensions on the same layer. Both patches are capacitively excited by a centrally positioned probe-fed microstrip line. The antenna occupies a compact size of $0.52\,\lambda \times 0.52\,\lambda \times 0.03\,\lambda$ at the lowest operating frequency of 5.2 GHz. Experimental results demonstrate that the proposed design achieve balanced performance in two bands. The measured impedance bandwidths are 6.1% and 4.9% for the lower and upper bands, respectively. Across these operating bands, the antenna achieves peak broadside gains of 7.0 and 6.7 dBi, and the front-to-back ratio is about 20 dB.

The associate editor coordinating the review of this manuscript and approving it for publication was Roberto S. Murphy (*Corresponding author: Nguyen Tran*).

T. Le-Tuan, H. Nguyen-Thi, and Nguyen Tran are with the Faculty of Electrical and Electronic Engineering, PHENIKAA School of Engineering, PHENIKAA University, Hanoi 12116, Vietnam (e-mails: 24100593@st.phenikaa-uni.edu.vn, tu.letuan@phenikaa-uni.edu.vn, and nguyen.tranvietduc@phenikaa-uni.edu.vn).

P. Hyun-chang is with the Division of Electronics & Electrical Engineering, Dongguk University, Seoul, Korea (e-mail: hcpark@dongguk.edu).

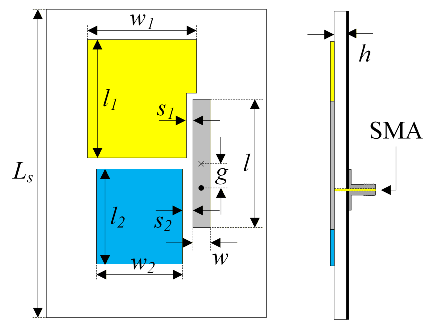

Fig. 1. Geometry of the initial dual-band antenna.

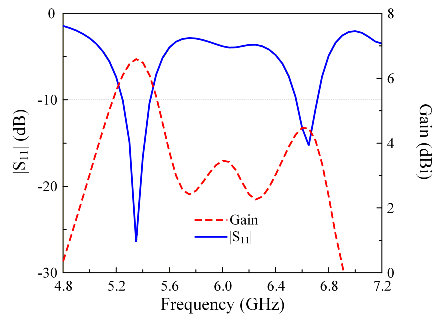

Fig. 2. Simulated $|S_{11}|$ and broadside gain of the initial dual-band antenna.

II. Dual-Band Antenna

A. Antenna Design

The geometrical configuration of the dual-band antenna is depicted in Fig. 1. The antenna is realized on a Taconic RF-35 substrate with a moderate dielectric constant (ε_r = 3.5), low loss tangent (approximately 0.0018). The moderate permittivity helps reduce the antenna size without causing excessive dielectric loss, while the low-loss property supports high gain and stable radiation performance. Dual-band operation is realized by integrating two radiating patches. The larger patch is designed to resonate at the lower frequency band, while the smaller patch is proportionally scaled to operate at the higher band. Both patches are electromagnetically excited through capacitive coupling from a probe-fed microstrip line that serves as the driven element. The resonant lengths of these patches (l_1 and l_2) are chosen about half-effective wavelength at the desired frequencies.

The antenna is modeled and analyzed using the full-wave electromagnetic solver Ansys High-Frequency Structure Simulator (HFSS). The optimal dimensions are $L_s = 35$, $h = 1.52$, $w = 2.0$, $l = 14.6$, $g = 2.6$, $s_1 = 0.7$, $s_2 = 1.2$, $l_1 = 13.5$, $w_1 = 12.5$, $l_2 = 10.8$, $w_2 = 9.8$ (unit: mm).

B. Antenna Performance

Fig. 2 presents the simulated reflection coefficient ($|S_{11}|$) and broadside gain of the dual-band antenna. As seen, two distinct resonance modes centered at approximately 5.35 GHz and 6.6 GHz are observed. The corresponding -10 dB impedance bandwidths are 5.25–5.45 GHz and 6.55–6.72 GHz, yielding fractional bandwidths of 3.7% and 2.6%. The realized broadside gain shown in Fig. 2 demonstrates that the antenna exhibits a stable gain response of 6.0–6.6 dBi in the lower band and 4.0–4.6 dBi in the upper band.

To verify the independent controllability of the two resonant bands, Fig. 3 present the simulated $|S_{11}|$ responses for varying patch lengths l_1 and l_2. Increasing l_1 shifts the lower resonant frequency downward due to the extended effective current path, while the upper band remains nearly unaffected. Conversely, adjusting l_2 primarily tunes the higher-frequency resonance with minimal impact on the lower band. Overall, the weak cross-sensitivity confirms that each band is mainly controlled by its corresponding patch dimension, enabling independent tuning of the dual-band operation.

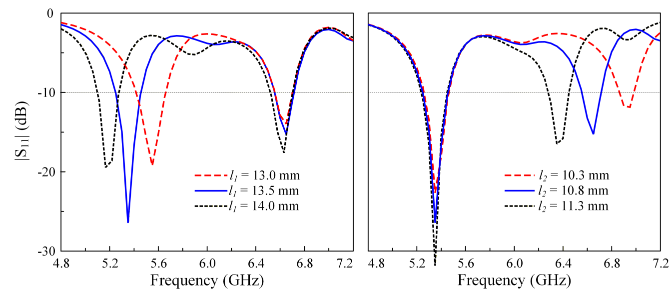

Fig. 3. Simulated $|S_{11}|$ of the initial dual-band antenna for different l_1 and l_2.

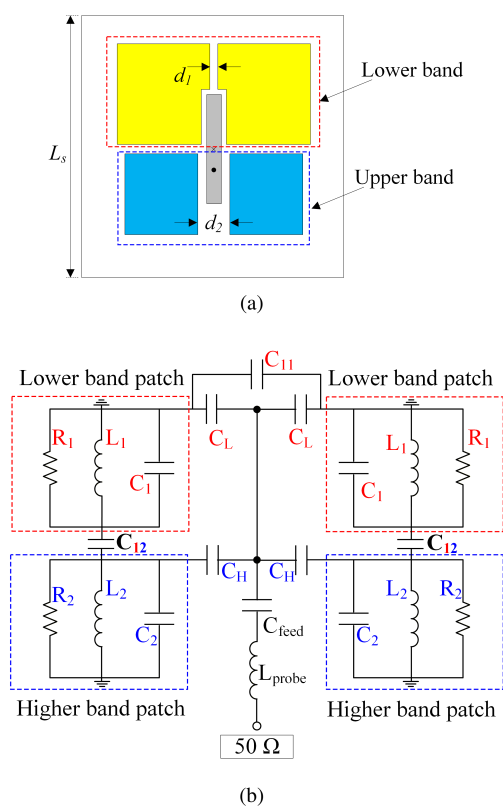

Fig. 4. (a) Geometry and (b) equivalent circuit of the proposed dual-band antenna.

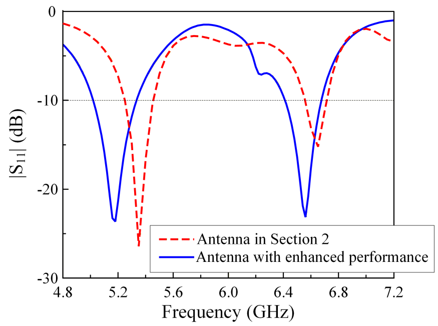

Fig. 5. Simulated $|S_{11}|$ the proposed dual-band antenna.

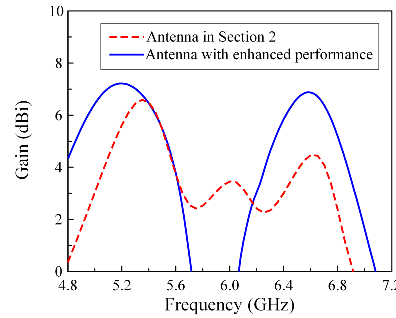

Fig. 6. Simulated broadside gain of the proposed dual-band antenna.

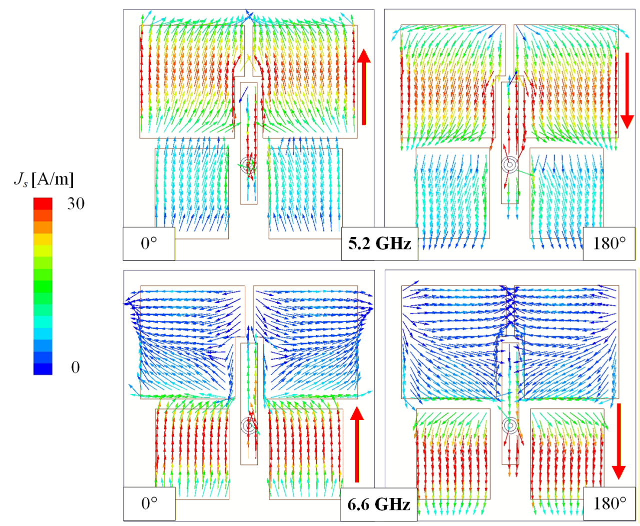

Fig. 7. Simulated surface current distributions of the proposed dual-band antenna.

III. Dual-Band Antenna with Enhanced Performance

A. Antenna Design

The dual-band antenna discussed in Section 2 suffers from narrow fractional bandwidths and limited broadside gain at both bands. For bandwidth and gain enhancement, more patches are employed, as illustrated in Fig. 4. The optimal dimensions are as follows: $L_s = 30$, $h = 1.52$, $w = 2.0$, $l = 14.6$, $g = 2.6$, $s_1 = 0.7$, $s_2 = 1.4$, $l_1 = 13.5$, $w_1 = 12.5$, $l_2 = 10.8$, $w_2 = 8.8$, $d_1 = 1.0$, $d_2 = 4.8$ (unit: mm). The equivalent circuit of the dual-band antenna is also shown in Fig. 4b. Each patch is modeled as a parallel resonant RLC circuit. Due to the similar structure, two patches for lower band operation are modeled as $R_1L_1C_1$, while those for higher band are $R_2L_2C_2$. These patches are excited with the coupling capacitances C_L and C_H. Due to the close proximity between two patches at lower and higher bands, their capacitance are C_{11} and C_{22}. Additionally, the coupling between the lower-band and higher-band patches is equivalent to capacitance C_{12}.

B. Antenna Operation Characteristics

The dual-band antenna discussed in Section 2 has narrow fractional bandwidths of 3.7% and 2.6% at lower and higher bands. Besides, the realized broadside gains are also limited, which are stable around 6.3 dBi in the lower band and 4.3 dBi in the upper band. When more patches are employed, Fig. 5 indicates that the operating bandwidth at the lower band is 6.2% (5.02–5.34 GHz), while the bandwidth for higher band is 4.2% (6.41–6.68 GHz). In terms of broadside gain shown in Fig. 6, the peak gain value at the lower band increases from 6.6 to 7.2 dBi, while that at the upper band enhances from 4.6 to 6.9 dBi. Adding one more patch for each band increases the effective radiating aperture and introduces a stronger distributed resonant region while preserving the same single metal layer. Therefore, the bandwidth and gain can be improved.

The dual-band mechanism is confirmed by observing the current distributions at the corresponding resonances. As shown in Fig. 7, the current at 5.2 GHz is predominantly concentrated on the larger patch, while only weak excitation is observed on the smaller patch. Conversely, at 6.6 GHz the current is mainly confined to the smaller patch, with negligible distribution on the larger one. This distinct current localization confirms that each patch independently supports its respective fundamental resonance, thereby validating the dual-band operation of the proposed design.

Among the key parameters governing the optimization of the proposed antenna, the gap between the radiating patches and the feeding microstrip line plays a dominant role. Fig. 8 shows the simulated $|S_{11}|$ responses for different values of d_1 and d_2. Increasing these values increases the physical separation between the feed line and the patch, thereby modifying the capacitive coupling strength between them. Consequently, the impedance matching in the higher-frequency band is highly sensitive to variations in d_2. In contrast, the lower frequency band is strongly affected by d1. Besides, the simulated results indicate that the two operating bands can be optimized with a high degree of independence.

IV. Measurement Results

The proposed antenna was fabricated and experimentally characterized. Fig. 9 shows photographs with respect to top- and bottom-view of the fabricated prototype. The reflection coefficient is measured with Vector Network Analyzer, while the far-field performance is characterized in an anechoic chamber. In the proposed design, the gaps between the patches and the center excitation are important. The results in Fig. 8 indicate that the antenna maintains good matching performance even

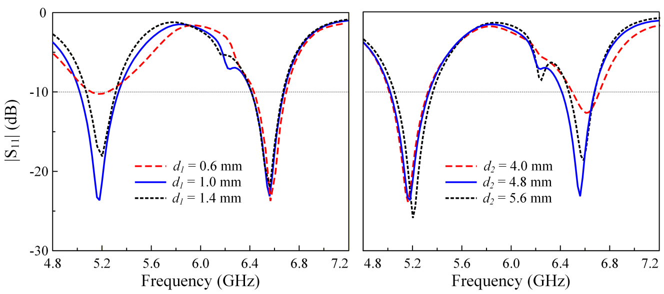

Fig. 8. Simulated $|S_{11}|$ of the proposed dual-band antenna for different values of d_1 and d_2.

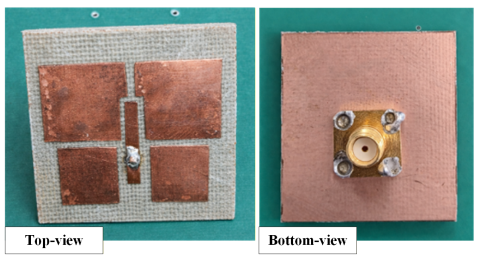

Fig. 9. Photographs of the fabricated antenna prototype.

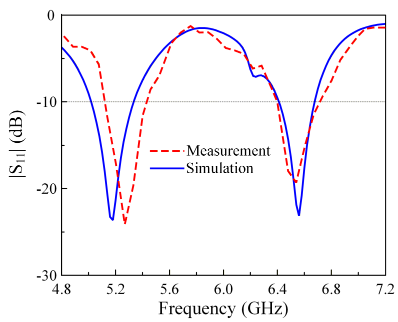

Fig. 10. Simulated and measured $|S_{11}|$ of the proposed dual-band antenna.

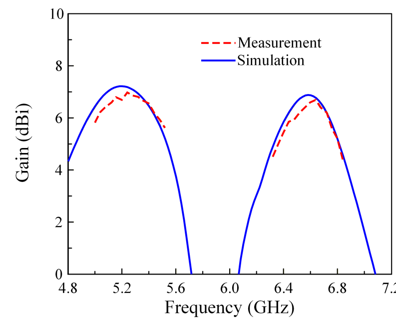

Fig. 11. Simulated and measured broadside gain of the proposed dual-band antenna.

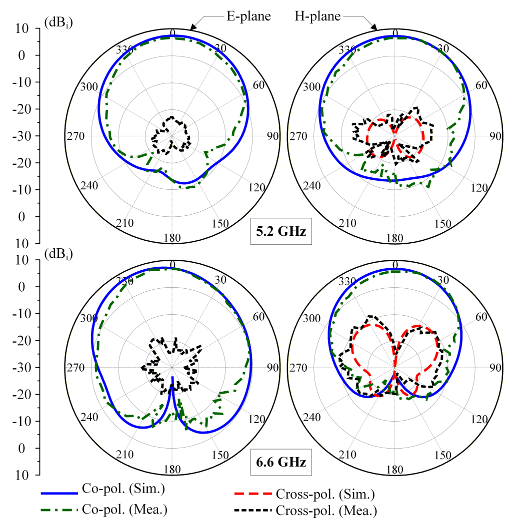

Fig. 12. Simulated and measured gain radiation pattern of the proposed antenna.

with a relatively large variation of d_1 and d_2, up to 0.8 mm. In practical PCB fabrication, the tolerance of wet etching is typically on the order of $\pm$0.05-0.1 mm, depending on the fabrication facility, copper thickness, substrate material, mask quality, and etching control. Since this practical tolerance is much smaller than the investigated dimensional variation, the proposed antenna is not highly sensitive to fabrication tolerances.

Overall, the measured results agree well with the simulations. Discrepancies between the simulated and measured gains are observed at both operating bands. These differences can be mainly attributed to fabrication tolerances and measurement uncertainties. Fig. 10 compares the simulated and measured reflection coefficients of the dual-band antenna. The measured lower-band impedance bandwidth is 6.1%, covering 5.12–5.44 GHz, while the upper band achieves 4.9% bandwidth from 6.40 to 6.72 GHz. Fig. 11 presents the simulated and measured broadside gains. The measured gain ranges from 6.2 to 7.0 dBi across the lower operating band around 5.2 GHz, whereas it varies from 5.4 to 6.7 dBi over the upper band. Further investigation also shows that the antenna can achieve high radiation efficiency of better than 88% at both bands.

The simulated and measured radiation gain patterns at the two frequencies corresponding to the dual-band operation are shown in Fig. 12. It is evident that the antenna maintains good radiation performance at both frequencies. The antenna exhibits stable linear polarization with very low cross-polarization levels, which are approximately 25 dB lower than the co-polarized component. In addition, the front-to-back ratio is relatively high, around 20 dB, indicating good directional broadside radiation.

V. Performance Comparison

To highlight the merits of the proposed dual-band antenna, a performance comparison with representative designs is summarized in Table I. It is evident that the use of multilayer configurations is a major drawback of the antennas reported in [5], [7]–[9], and [12], as it increases structural complexity and fabrication difficulty. Compared with existing single-layer counterparts, the proposed antenna achieves favorable impedance bandwidth and gains in both operating bands while maintaining a compact footprint. In addition, a high front-to-back ratio (FBR) is another distinct advantage over

TABLE I
PERFORMANCE COMPARISON AMONG DUAL-BAND PATCH ANTENNAS

Ref.	**Overall size** (λ)	**No. of layers**	**Bandwidth (%)** f_L	f_H	**Peak gain (dBi)** f_L	f_H	**FBR (dB)**
[5]	$1.28 \times 0.71 \times 0.02$	2	2.1	4.4	3.0	9.0	20
[7]	$0.82 \times 0.82 \times 0.06$	5	13.1	12.8	9.1	8.6	20
[8]	$0.80 \times 0.80 \times 0.02$	3	< 1.0	< 2.0	N/G	N/G	N/G
[9]	$0.62 \times 0.62 \times 0.06$	2	5.3	24.1	2.2	4.0	12
[12]	$0.58 \times 0.51 \times 0.05$	2	3.3	22.4	5.1	5.2	11
[13]	$0.43 \times 0.36 \times 0.02$	1	< 3.0	< 3.0	6.2	5.1	10
[14]	$1.56 \times 1.08 \times 0.05$	1	9.0	5.0	6.0	8.0	10
[15]	$0.32 \times 0.19 \times 0.01$	1	4.0	2.2	1.0	2.4	10
[17]	$0.16 \times 0.15 \times 0.01$	1	< 1.0	15.4	-1.7	2.4	8
[18]	$0.47 \times 0.35 \times 0.03$	1	11.4	4.5	3.8	2.0	15
[19]	$1.13 \times 0.47 \times 0.02$	1	3.1	19.0	8.9	13.6	15
[20]	N/G	1	< 1.0	< 3.0	2.6	6.6	10
[21]	$0.52 \times 0.52 \times 0.02$	1	1.2	1.1	5.6	11.4	N/G
Prop.	$0.52 \times 0.52 \times 0.03$	1	6.1	4.9	7.0	6.7	20

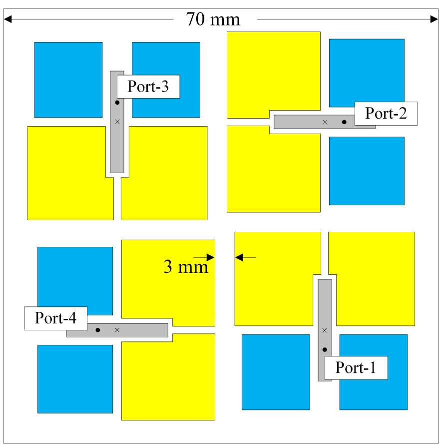

Fig. 13. Geometry of the 4×4 MIMO antenna.

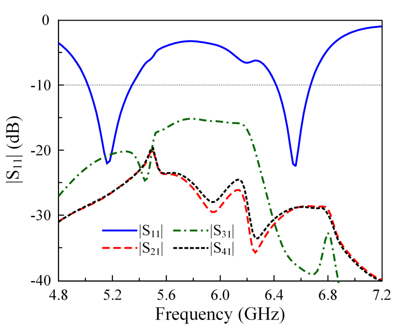

Fig. 14. Simulated S-parameter of the 4×4 MIMO antenna.

the compared designs. Although smaller antenna sizes are reported in [13], [15], [17], and [18], these works generally suffer from lower gain and/or narrower bandwidth than the proposed design. The antenna in [19] provides higher gain than the proposed work. Nonetheless, its overall dimensions are significantly larger due to the use of multiple radiating elements.

VI. MIMO CONFIGURATION

To enhance the channel capacity, MIMO configuration is considered [22], [23]. Fig. 13 shows the geometry of the

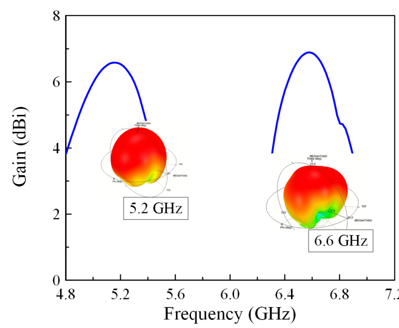

Fig. 15. Simulated broadside gain of the 4×4 MIMO antenna.

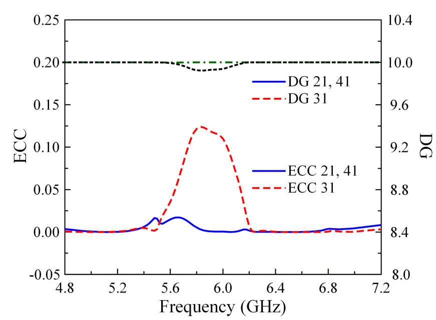

(a)

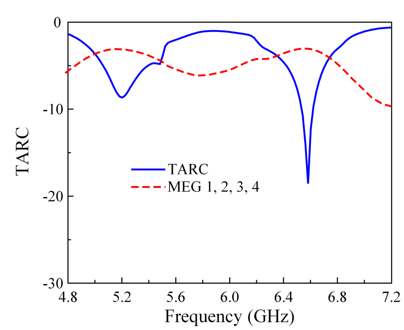

(b)

Fig. 16. Calculated (a) ECC, DG, and (b) TARC, MEG of the MIMO antenna.

proposed 4×4 MIMO configuration. Here, four dual-band elements are arranged in 2×2 configurations. They are positioned orthogonally to achieve high isolation. Besides, the MIMO antenna can achieve both polarization and spatial diversity. The edge-to-edge spacing is small, about 3 mm, corresponding to about 0.05λ at 5.2 GHz. Fig. 14 shows the simulated S-parameter of the MIMO antenna. As seen, the operating bandwidths are 6.4% (5.02–5.35 GHz) and 4.0% (6.41–6.67 GHz) at the lower and upper bands, respectively. Across these bands, the port isolations are always higher than 20 dB. In fact, larger spacing would improve isolation at the cost of a larger footprint. In terms of gain depicted in Fig. 15, the peak gains are 6.6 and 6.9 dBi at lower band and higher band. The results demonstrate the good operating performance of the proposed MIMO antenna.

The MIMO diversity performance in terms of Envelop Correlation Coefficient (ECC), Diversity Gain (DG), Total Active Reflection Coefficient (TARC), and Mean Effective Gain (MEG) is considered. The calculated ECC, DG, TARC, and MEG results are depicted in Fig. 16. The results show ECC below 0.02, DG higher than 9.9 dB, acceptable TARC over the operating bands, balanced MEG among the ports, confirming good diversity performance.

VII. Conclusion

This work has presented a compact single-layer dual-band patch antenna for WiFi 6/6E communication systems. By integrating multiple closely spaced patches of different sizes on the same layer and employing capacitive coupling through a centrally located probe-fed microstrip line, the proposed design achieves dual-band performance with a low-profile and highly compact structure. The antenna occupies only $0.52\,\lambda \times 0.52\,\lambda \times 0.03\,\lambda$ at 5.2 GHz, demonstrating the advantage of the proposed single-layer miniaturized configuration. Measured results confirm bandwidths of 6.1% and 4.9% for the lower and upper bands, respectively, with corresponding peak broadside gains of 7.0 and 6.7 dBi. In addition, the antenna maintains stable radiation characteristics with high FBR of 20 dB across both operating bands, validating its effectiveness as a compact dual-band solution.

References

[1] U. Musa, S. M. Shah, H. A. Majid, I. A. Mahadi, M. K. A. Rahim, M. S. Yahya, and Z. Z. Abidin, "Design and implementation of active antennas for iot-based healthcare monitoring system," *IEEE Access*, vol. 12, pp. 48 453–48 471, 2024. doi: 10.1109/access.2024.3384371

[2] R. K. Verma, D. K. Srivastava, R. P. Tripathi, and V. Rajpoot, "Wide dual band asymmetrical i-shape rectangular microstrip patch antenna for pcs/umts/wimax/imt applications," *Wireless Personal Communications*, vol. 122, no. 2, pp. 1577–1598, Aug. 2021. doi: 10.1007/s11277-021-08962-7

[3] S. X. Ta and I. Park, "Dual-band low-profile crossed asymmetric dipole antenna on dual-band amc surface," *IEEE Antennas and Wireless Propagation Letters*, vol. 13, pp. 587–590, 2014. doi: 10.1109/lawp.2014.2312950

[4] H. Zhai, K. Zhang, S. Yang, and D. Feng, "A low-profile dual-band dual-polarized antenna with an amc surface for wlan applications," *IEEE Antennas and Wireless Propagation Letters*, vol. 16, pp. 2692–2695, 2017. doi: 10.1109/lawp.2017.2741465

[5] N.-W. Liu, S. Gao, G. Fu, and L. Zhu, "A low-profile dual-band patch antenna with simultaneous wide beamwidth and high gain by using multiresonant modes," *IEEE Antennas and Wireless Propagation Letters*, vol. 20, no. 5, pp. 813–817, May 2021. doi: 10.1109/lawp.2021.3064263

[6] C. X. Mao, S. Gao, Y. Wang, B. Sanz-Izquierdo, Z. Wang, F. Qin, Q. X. Chu, J. Li, G. Wei, and J. Xu, "Dual-band patch antenna with filtering performance and harmonic suppression," *IEEE Transactions on Antennas and Propagation*, vol. 64, no. 9, pp. 4074–4077, Sep. 2016. doi: 10.1109/tap.2016.2574883

[7] J. Hao, N. Yan, Y. Luo, H. Fu, and K. Ma, "A low-cost dual-band multimode high-gain stacked-patch antenna based on sisl for 5g applications," *IEEE Antennas and Wireless Propagation Letters*, vol. 21, no. 1, pp. 4–8, Jan. 2022. doi: 10.1109/lawp.2021.3112459

[8] H. Zhang, L. Chang, and A. Zhang, "Low-profile and dual-band microstrip patch antenna based on magnetic coupling covering wi-fi 6 bands for mobile terminals," *IEEE Antennas and Wireless Propagation Letters*, vol. 24, no. 7, pp. 1899–1903, Jul. 2025. doi: 10.1109/lawp.2025.3550499

[9] C. Y. Chiu, C. H. Chan, and K. M. Luk, "Small dual-band antenna with folded-patch technique," *IEEE Antennas and Wireless Propagation Letters*, vol. 3, pp. 108–110, 2004. doi: 10.1109/lawp.2004.830025

[10] X.-Q. Zhu, Y.-X. Guo, and W. Wu, "Miniaturized dual-band and dual-polarized antenna for mban applications," *IEEE Transactions on Antennas and Propagation*, vol. 64, no. 7, pp. 2805–2814, Jul. 2016. doi: 10.1109/tap.2016.2556701

[11] B. Shi and C. Deng, "28/38 ghz single-feed stacked patch antenna for 5g communication," in *2019 International Conference on Microwave and Millimeter Wave Technology (ICMMT)*. IEEE, May 2019, pp. 1–3. doi: 10.1109/icmmt45702.2019.8992586

[12] S. Li, W. Lu, and L. Zhu, "Dual-band stacked patch antenna with wide e-plane beam width and stable gain at both bands," *Microwave and Optical Technology Letters*, vol. 63, no. 4, pp. 1264–1270, Nov. 2020. doi: 10.1002/mop.32731

[13] M. Wei, J. Wang, X. Wang, T. Liu, Y. Lu, and Y. Gao, "Low-profile dual-band microstrip patch antenna with shorting pins," *IEEE Antennas and Wireless Propagation Letters*, vol. 23, no. 6, pp. 1834–1838, Jun. 2024. doi: 10.1109/lawp.2024.3370724

[14] N.-W. Liu, L. Zhu, Z.-X. Liu, and Y. Liu, "Dual-band single-layer microstrip patch antenna with enhanced bandwidth and beamwidth based on reshaped multiresonant modes," *IEEE Transactions on Antennas and Propagation*, vol. 67, no. 11, pp. 7127–7132, Nov. 2019. doi: 10.1109/tap.2019.2927646

[15] A. Jafargholi, A. Jafargholi, and B. Ghalamkari, "Dual-band slim microstrip patch antennas," *IEEE Transactions on Antennas and Propagation*, vol. 66, no. 12, pp. 6818–6825, Dec. 2018. doi: 10.1109/tap.2018.2871964

[16] W. C. Mok, S. H. Wong, K. M. Luk, and K. F. Lee, "Single-layer single-patch dual-band and triple-band patch antennas," *IEEE Transactions on Antennas and Propagation*, vol. 61, no. 8, pp. 4341–4344, Aug. 2013. doi: 10.1109/tap.2013.2260516

[17] A. A. Salih and M. S. Sharawi, "A dual-band highly miniaturized patch antenna," *IEEE Antennas and Wireless Propagation Letters*, vol. 15, pp. 1783–1786, 2016. doi: 10.1109/lawp.2016.2536678

[18] X.-H. Ding, Z. Tan, and S. N. Burokur, "A compact single layer dual band microstrip patch antenna for 5g terminal applications," *Scientific Reports*, vol. 15, no. 1, Mar. 2025. doi: 10.1038/s41598-025-93592-3

[19] Y. Q. Guo, Y. M. Pan, S. Y. Zheng, and K. Lu, "A singly-fed dual-band microstrip antenna for microwave and millimeter-wave applications in 5g wireless communication," *IEEE Transactions on Vehicular Technology*, vol. 70, no. 6, pp. 5419–5430, Jun. 2021. doi: 10.1109/tvt.2021.3070807

[20] B. P. Smyth, S. Barth, and A. K. Iyer, "Dual-band microstrip patch antenna using integrated uniplanar metamaterial-based ebgs," *IEEE Transactions on Antennas and Propagation*, vol. 64, no. 12, pp. 5046–5053, Dec. 2016. doi: 10.1109/tap.2016.2618854

[21] C. Arora, S. S. Pattnaik, and R. Baral, "Dual band microstrip patch antenna array loaded with split ring resonators and via holes," *AEU - International Journal of Electronics and Communications*, vol. 93, pp. 253–260, Sep. 2018. doi: 10.1016/j.aeue.2018.06.016

[22] R. Jain, V. V. Thakare, and P. K. Singhal, "Design and comparative analysis of thz antenna through machine learning for 6g connectivity," *IEEE Latin America Transactions*, vol. 22, no. 2, pp. 82–91, 2024. doi: 10.1109/TLA.2024.10412032

[23] R. R, R. V, and R. Jain, "Machine learning assisted mm-wave mimo antenna design with high isolation for 5g applications," *IEEE Latin America Transactions*, vol. 23, no. 12, pp. 1325–1334, 2025. doi: 10.1109/TLA.2025.11231218

Tu Le-Tuan received his B.S. degree in electronics and telecommunications from Hanoi University of Science and Technology, Hanoi, Vietnam, in 2013, and the Ph.D. degree from the Department of Electronics and Electrical Engineering, Dongguk University, Seoul, South Korea. His current research interests include RF energy harvesting, wearable antennas, circularly polarized antennas, reconfigurable antennas, and multiband/broadband planar antennas for various wireless applications.

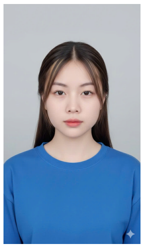

Hien Nguyen-Thi is currently pursuing her B.S. degree in Electrical and Electronics Engineering at PHENIKAA University, Hanoi, Vietnam. She is currently in her second year of undergraduate studies. Her research interests focus on applied electromagnetics and advanced antenna design, with a particular emphasis on wideband microstrip patch antennas, MIMO systems, and the integration of metasurfaces for 5G communications and Internet of Things (IoT) applications.

Nguyen Tran received a B.S. degree in Communication Command at Telecommunications University, Vietnam, in 2011. He received his M.S. degree in Electronics Engineering from Le Quy Don Technical University, Vietnam in 2017. He is currently an Assistant with Phenikaa University, Hanoi, Vietnam. His research interests are centered on antenna design and RF engineering, specifically focusing on the optimization of microstrip patch antennas and the development of wideband systems. His work also explores the implementation of circular polarization, metasurfaces for bandwidth enhancement on MIMO antennas.

Hyun-Chang Park (Member, IEEE) received his B.S. degree in electronics engineering from Seoul National University, Seoul, South Korea, in 1986, and the M.S. and Ph.D. degrees in electrical engineering from Cornell University, Ithaca, NY, USA, in 1989 and 1993, respectively. From 1993 to 1995, he was a Research Associate with the Department of Electrical Engineering, University of Virginia, Charlottesville, VA, USA. In 1995, he joined the Department of Electronics and Electrical Engineering, Dongguk University, Seoul, South Korea, where he is currently a Professor. His research interests include RF energy harvesting, wideband/multi-band planar antennas, and reconfigurable antennas for various wireless applications.